


Article

Performance Optimization and Toxicity Effects of the Electrochemical Oxidation of Octogen

Yishi Qian^{1,2}, Kai Chen³, Guodong Chai³, Peng Xi², Heyun Yang³, Lin Xie³, Lu Qin³, Yishan Lin⁴, Xiaoliang Li³, Wei Yan^{1,*} and Dongqi Wang^{3,5,6,*} 

- ¹ Department of Environmental Science and Engineering, School of Energy and Power Engineering, Xi'an Jiaotong University, Xi'an 710049, China; qys1017@stu.xjtu.edu.cn
- ² Xi'an Modern Chemistry Research Institute, Xi'an 710065, China; pengxi204@outlook.com
- ³ Department of Municipal and Environmental Engineering, School of Water Resources and Hydro-Electric Engineering, Xi'an University of Technology, Xi'an 710048, China; 3180673038@xtu.xaut.edu.cn (K.C.); xaut_chaigd@yahoo.com (G.C.); heyunyang.xaut@yahoo.com (H.Y.); 1170411051@xtu.xaut.edu.cn (L.X.); 2200421182@xtu.xaut.edu.cn (L.Q.); lixiaoliang@xaut.edu.cn (X.L.)
- ⁴ State Key Laboratory of Pollution Control & Resource Reuse, School of the Environment, Nanjing University, Nanjing 210023, China; yshanlisa@nju.edu.cn
- ⁵ State Key Laboratory of Eco-Hydraulics in Northwest Arid Region, Xi'an University of Technology, Xi'an 710048, China
- ⁶ Shaanxi Key Laboratory of Water Resources and Environment, Xi'an University of Technology, Xi'an 710048, China
- * Correspondence: yanwei@mail.xjtu.edu.cn (W.Y.); wangdq@xaut.edu.cn (D.W.)

Abstract: Octogen (HMX) is widely used as a high explosive and constituent in plastic explosives, nuclear devices, and rocket fuel. The direct discharge of wastewater generated during HMX production threatens the environment. In this study, we used the electrochemical oxidation (EO) method with a PbO₂-based anode to treat HMX wastewater and investigated its degradation performance, mechanism, and toxicity evolution under different conditions. The results showed that HMX treated by EO could achieve a removal efficiency of 81.2% within 180 min at a current density of 70 mA/cm², Na₂SO₄ concentration of 0.25 mol/L, interelectrode distance of 1.0 cm, and pH of 5.0. The degradation followed pseudo-first-order kinetics ($R^2 > 0.93$). The degradation pathways of HMX in the EO system have been proposed, including cathode reduction and indirect oxidation by •OH radicals. The molecular toxicity level (expressed as the transcriptional effect level index) of HMX wastewater first increased to 1.81 and then decreased to a non-toxic level during the degradation process. Protein and oxidative stress were the dominant stress categories, possibly because of the intermediates that evolved during HMX degradation. This study provides new insights into the electrochemical degradation mechanisms and molecular-level toxicity evolution during HMX degradation. It also serves as initial evidence for the potential of the EO-enabled method as an alternative for explosive wastewater treatment with high removal performance, low cost, and low environmental impact.

Keywords: electrochemistry; octogen; wastewater; hydroxyl radical; toxicity



Citation: Qian, Y.; Chen, K.; Chai, G.; Xi, P.; Yang, H.; Xie, L.; Qin, L.; Lin, Y.; Li, X.; Yan, W.; et al. Performance Optimization and Toxicity Effects of the Electrochemical Oxidation of Octogen. *Catalysts* **2022**, *12*, 815. <https://doi.org/10.3390/catal12080815>

Academic Editors: Hao Xu and Yanbiao Liu

Received: 20 June 2022

Accepted: 21 July 2022

Published: 25 July 2022

Publisher's Note: MDPI stays neutral with regard to jurisdictional claims in published maps and institutional affiliations.



Copyright: © 2022 by the authors. Licensee MDPI, Basel, Switzerland. This article is an open access article distributed under the terms and conditions of the Creative Commons Attribution (CC BY) license (<https://creativecommons.org/licenses/by/4.0/>).

1. Introduction

Octogen [octahydro-1,3,5,7-tetranitro-1,3,5,7-tetrazocine (HMX)] is a highly explosive material widely used in plastic explosives, nuclear devices, rocket fuel, and other products [1]. As a heterocyclic compound with an eight-membered ring, HMX exhibits higher stability and detonation capacity than other conventional explosives [2,4,6-trinitrotoluene, hexahydro-1,3,5-trinitro-1,3,5-triazine (RDX)]. However, HMX poses potential threats to soil microorganisms, plants, animals, and humans [2]. It damages the central nervous, renal, and hepatic systems of mice and rats when oral exposure levels exceed 200 mg/kg [3]. HMX can also enter the human body through inhalation, dermal contact, and diet, inducing adverse effects on the central nervous system [4]. The US Environmental Protection

Agency (EPA) recommends that cumulative human exposure to HMX should not exceed 400 µg/L [4]. Owing to the persistent and non-degradable nature of HMX, it may leak into the surrounding water and soil during production, storage, and application. Continuous accumulation in the environment may impact living organisms [5] and affect the functioning of ecosystems [6]. Therefore, methods for the effective removal of HMX are urgently required.

Biological and physical methods are typically used to treat HMX wastewater. Although physical methods (e.g., membrane separation and reverse osmosis) are effective and easy to perform, they are expensive and can cause secondary pollution [7,8]. Biological treatments are the most economical method by which to remove readily biodegradable organic matter from wastewater. However, high levels of persistent organic matter and toxic substances, such as HMX, greatly reduce the efficiency of biological treatments [9–11]. Zhao et al. [12] conducted in situ HMX degradation in low-temperature marine sediments under anaerobic conditions and found that 50 days were required to degrade 50% of the HMX. Kanekar et al. [13] investigated the potential of soil yeast (*Pichia sydowiorum* MCM Y-3) to treat HMX wastewater in a fixed-film bioreactor (FFBR) and found that only 28–50% of the HMX was removed (HRT of one week). Therefore, it is crucial to choose a method that can effectively degrade HMX with a low environmental impact. Advanced oxidation processes (AOPs) can improve the biodegradability of wastewater while simultaneously treating pollutants [14,15]. Among these processes, the electrochemical oxidation (EO) process, which utilizes a cathode and anode to convert electric energy into chemical energy under an external electric field, has been widely used to treat organic wastewater that is difficult to biodegrade [16]. The EO method can be divided into direct and indirect oxidation reactions [17]. During direct oxidation, pollutants are adsorbed onto the anode surface and then oxidized into small-molecule organic matter. Indirect oxidation involves the oxidation of organic pollutants through the formation of strongly oxidizing intermediates, such as hydroxyl radicals ($\bullet\text{OH}$), chlorate, ozone, and hydrogen peroxide, during the electrochemical reaction [18,19]. Because the EO method can completely oxidize organic pollutants in wastewater and results in lower chemical oxygen demand (COD) and toxicity [20,21], it can be promising for explosive wastewater treatment [22]. Recent studies have revealed that RDX-containing wastewater can be effectively treated by using EO process, resulting in 39.2% COD removal and 97.5% RDX removal, as well as significantly increased biodegradability [16]. A previous study by Bonin et al., elucidated the capability of an EO system with a boron-doped diamond (BDD) electrode to treat three nitramine explosives (RDX, HMX, and 2,4,6,8,10,12-hexanitro-2,4,6,8,10,12-hexaazaisowurtzitane (CL-20)) [23]. However, the high cost of BDD anodes limits their large-scale industrial application [24]. Instead, PbO_2 -based anodes have been widely used in many EO systems and are considered a valid alternative to BDD electrodes because of their good conductivity, favorable overpotential, high chemical inertness, low cost, and excellent electrocatalytic performance [25–28]. Nonetheless, the application of the PbO_2 electrode-based EO system for HMX wastewater treatment and its optimal operating conditions (e.g., pH and current density) have not been well studied.

Moreover, limited research has focused on the HMX degradation mechanisms. Analyzing the intermediates of HMX is essential to understand its degradation pathway. Under anaerobic conditions, nitro derivatives are the intermediates formed by the reduction of the nitro groups on the HMX ring [11,29], mainly forming octahydro-1-nitroso-3,5,7-trinitro-1,3,5,7-tetrazocine (1NO-HMX) or octahydro-1,5-dinitroso-3,7-dinitro-1,3,5,7-tetrazocine (2NO-HMX) [29,30]. HMX can be converted to the ring-cleavage products, methylene nitramine, and bis(hydroxymethyl)nitramine, which are subsequently converted to formaldehyde, formic acid, and nitrous oxide [11,30]. However, the electrochemical degradation pathways of HMX have not been studied extensively. In addition, previous studies regarding the toxicity of energy-containing materials (e.g., RDX and HMX) are mostly based on cellular and mammalian bioassays [31,32], and little is known about molecular-level toxicity effects. Gou et al., recently developed a quantitative

toxicogenomics-based assay by using cellular stress response pathways to reveal the potential toxicity mechanisms of target toxicants at the transcriptional level [33]. Compared to conventional resource-intensive, animal-based and isolated bioassays, this high-throughput assay is more rapid and cost-effective and can capture diverse and perhaps overlapping modes of action (MOAs) resulting from trace-level chemicals or chemical mixtures. The assay has been successfully used to evaluate the toxic effects and safety of nanomaterials and drinking water [33,34] and is therefore considered suitable for the assessment of molecular toxicity evolution during HMX degradation.

Therefore, in this study, we used a Ti/PbO₂ electrode as the anode and a copper plate as the cathode to construct the EO system. The effects of different process parameters, including initial pH, current density, and electrode distance, on HMX degradation were studied. The energy consumption (EC) for HMX degradation was estimated at varying operating conditions. Performance optimization and intermediate analysis were conducted to reveal the EO reaction mechanism, providing critical data and guidance for the industrialization of HMX wastewater treatment. The toxicogenomics-based assay was performed to investigate molecular-level toxicity effects in order to assess the potential health risks of the treated effluent. The results provide new insights into the electrochemical degradation of HMX and support the development of an effective, economically feasible, and environmentally friendly method for explosive wastewater treatment.

2. Results and Discussion

2.1. Performance Optimization of HMX Degradation by Electrochemical Oxidation

2.1.1. Electrolyte Concentration

Na₂SO₄ is considered a good electrolyte owing to its stability [35]. The effect of Na₂SO₄ concentration on HMX removal was investigated at a current density of 30 mA/cm², HMX concentration of 20 mg/L, interelectrode distance of 1.5 cm, and pH of 7.0. As shown in Figure 1a, the HMX removal efficiency increased rapidly within 30 min; however it slowed down thereafter. When the Na₂SO₄ concentration increased from 0.05 to 0.25 mol/L, the HMX removal efficiency increased from 50.2% to 64.5%. Figure 1a and Table S1 show the linear regression of HMX removal over time during electrochemical degradation, where $\ln(C_0/C_t)$ increased linearly with time, confirming that electrochemical degradation follows pseudo-first-order kinetics.

Electrolytes, such as Na₂SO₄, can facilitate the transport of electrons and ions. Generally, the conductivity of the EO system increases with increasing electrolyte concentration, which promotes the production of reactive groups such as •OH, thus increasing the electrooxidation reaction rate [36]. In addition, SO₄²⁻ may be oxidized to S₂O₈²⁻, a powerful oxidizing agent that facilitates the oxidation of organic pollutants [16]. However, excess electrolyte concentrations lead to the accumulation of excess ions on the surface of the electrodes [37]. It will prevent the effective contact of organic contaminants, or produce unstable intermediates such as HO₂• radicals, which may be detrimental to the removal of persistent organic compounds [38]. As shown in Figure S1a, the cell voltage decreased with the increase of electrolyte concentrations so that the EC was saved. In this study, an Na₂SO₄ concentration of 0.25 mol/L was found to provide the highest HMX removal efficiency without adverse effects.

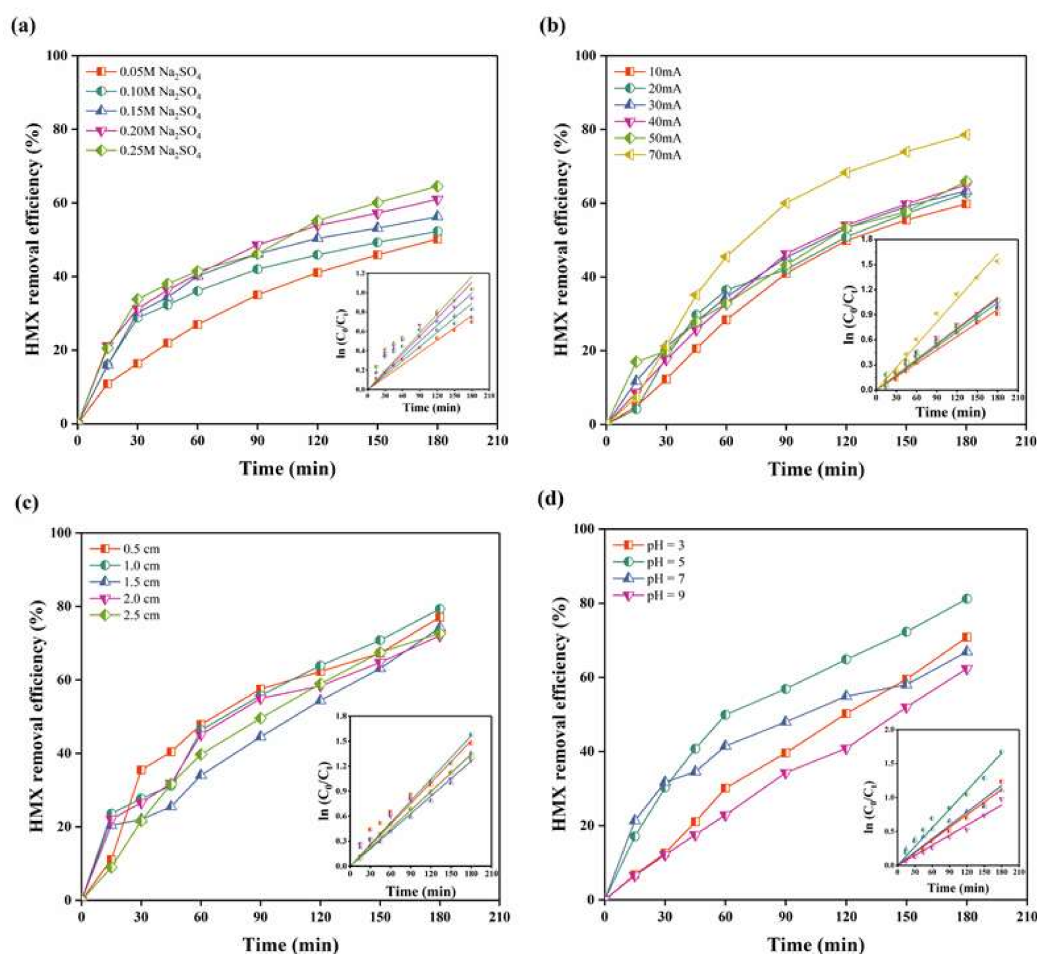


Figure 1. The effects of different operating parameters on HMX removal efficiency. (a) Electrolyte concentrations; (b) current densities; (c) electrode distance; (d) initial pH. The inset plot depicts corresponding pseudo-first-order kinetics.

2.1.2. Current Density

Several studies have concluded that increasing the current density in EO systems can improve the removal and mineralization efficiency of organic pollutants [39–41]. The effect of the current density on HMX removal was investigated at an electrolyte concentration of 0.25 mol/L, HMX concentration of 20 mg/L, interelectrode distance of 1.5 cm, and pH of 7.0. As shown in Figure 1b, HMX removal increased as the applied current density increased from 10 to 70 mA/cm². At a current density of 70 mA/cm², the HMX removal performance was significantly higher than that under other current density conditions. The HMX removal efficiency increased rapidly during the first 90 min, after which the rate of increase decreased, reaching a maximum removal efficiency of 78.6% at 180 min. Kinetic fitting of the HMX degradation curve at different current densities revealed a degradation rate constant of 5.4×10^{-2} to $9.0 \times 10^{-2} \text{ min}^{-1}$ (Table S1). Notably, the degradation rate of the contaminants increased slowly when the current density was increased from 10 to 50 mA/cm², whereas the degradation rate increased significantly when the current density was increased to 70 mA/cm².

Previous studies have reported that anodic oxidation is mass-transfer-controlled under low pollutants concentration or high current density conditions [42–44]. In this study, the initial HMX concentration was set constantly at 20 mg/L, resulting in the same and relatively limited mass transfer rate for all the tests. Therefore, the increase in the applied current density would not enhance the electrochemical oxidation rate of HMX significantly. Meanwhile, a continuous increase in the current density could lead to higher $\bullet\text{OH}$ production and electron transfer rate between the electrode surface and HMX molecules. Because

HMX is a heterocyclic nitramine whose structure is less electron-rich than the other aromatic nitramines, it is more difficult for $\bullet\text{OH}$ to attach to the heterocyclic compound [22,45]. Therefore, other degradation pathways (e.g., reduction on the cathode) rather than $\bullet\text{OH}$ radical oxidation should contribute more to HMX degradation when the current density increases to 70 mA/cm^2 , resulting in a higher degradation rate. The HMX removal performance may be improved with an even higher current density. However, the EC values largely increased from 0.50 to 4.47 kWh/g (Figure S1b and Table S3) due to the increasing voltage and enhanced side reaction. It would also result in higher carbon emissions, which is not feasible for real wastewater treatment. Therefore, the current density of 70 mA/cm^2 was deemed the optimal condition for the following experiments.

2.1.3. Interelectrode Distance

The effect of interelectrode distance on HMX removal was investigated at a current density of 70 mA/cm^2 , electrolyte concentration of 0.25 mol/L , HMX concentration of 20 mg/L , and pH of 7.0. Figure 1c shows that the interelectrode distance did not significantly affect the HMX removal efficiency, which was stable at approximately 75%. In general, the electric field intensity between the electrodes decreased with increasing interelectrode distance. The organic oxidation rate at the anode is faster with a shorter interelectrode distance, which may be attributed to better electrolytic performance at shorter diffusion distances [44]. When the interelectrode distance increased, the potential difference between the solution and anode decreased and weakened the driving force of the mass transfer. An increase in the mass transfer distance also reduces the concentration gradient of the solution and increases the resistance to mass transfer [46], thus leading to a decrease in the degradation performance. However, excessive reduction in the electrode distance leads to electrode breakdown or electrode short circuits [44,47]. Based on the obtained results (Figure 1c), an electrode plate spacing of 1.0 cm was considered optimal.

2.1.4. pH

The pH of the solution will affect the removal performance of organic pollutants in EO systems [48–50]. Strongly acidic (pH 3.0), acidic (pH 5.0), neutral (pH 7.0), and basic (pH 9.0) conditions were selected to assess the effect of pH on HMX removal (Figure 1d). After 180 min of EO treatment, the HMX removal efficiency reached 81.2% under acidic conditions (pH 5), whereas the efficiency was only 62.4% under alkaline conditions (pH 9). Kinetic fitting of the HMX degradation curves at different pH values revealed that the degradation rate constant was 4.9×10^{-2} to $9.2 \times 10^{-2}\text{ min}^{-1}$ (Table S1). It was observed that the oxidation potential of $\bullet\text{OH}$ was higher under acidic conditions (+2.85 V) than under basic conditions (+2.02 V) [51], suggesting that the EO system would have better pollutant treatment performance under acidic conditions. An increase in the solution pH reduces the oxygen evolution potential (OEP), facilitating the oxygen evolution reaction (OER), and thus reducing the pollutant removal efficiency [52]. Similar results were observed when the carbon felt/ PbO_2 anode was used for diuron degradation, and the highest efficiency was detected at lower pH values [53,54]. However, if the acidity is too strong, the hydrogen evolution reaction (HER) will be violent, which will also reduce the treatment performance [55] and the lifetime of the Ti/PbO_2 electrode [56]. Additionally, the changes in calculated EC values (Figure S1d) suggested that the initial pH of 5.0 was more favorable for both HMX degradation and cost savings.

2.2. Possible Electrochemical Degradation Mechanism of HMX

The electrochemical degradation intermediates of HMX were analyzed by using liquid chromatography-tandem mass spectrometry (LC–MS/MS). Table S2 and Figure S2 show the MS results for HMX intermediates within 180 min of EO treatment. Based on these results, two possible HMX degradation pathways were identified (Figure 2). In pathway A, the nitro group on HMX is reduced on the Cu cathode of the EO system to produce the mononitro derivative 1NO-HMX (intermediate I, $m/z = 281$), which is similar

to the previously reported microbial degradation mechanism of HMX [57]. Intermediate II ($m/z = 234$) contains an active imine bond (C=N) and is formed by N-denitration [58]. This intermediate reacts with water to form unstable α -hydroxy-alkylnitramine (intermediate III, $m/z = 252$) and then produces 4-nitro-2,4-diazabutanal (intermediate IV, $m/z = 120$), N_2O , and formaldehyde via ring cleavage [58]. In pathway B, the $\bullet OH$ generated by the EO process reacts with the carbon radical of HMX to generate hydroxyl-containing intermediate V ($m/z = 313$). Intermediate V would subsequently undergo ring cleavage to generate other intermediates such as methylene dinitramine and urea [59]. Both these by-products can be oxidized to form acetamide and formic acid, which continue to be oxidized, accompanied by the formation of NO_3^- and/or NH_4^+ . Although some of the small-molecule substances were not determined in this study, methylene dinitramine (intermediate VI, $m/z = 137$) was detected, which was also found in the HMX degradation process by municipal anaerobic sludge [30].

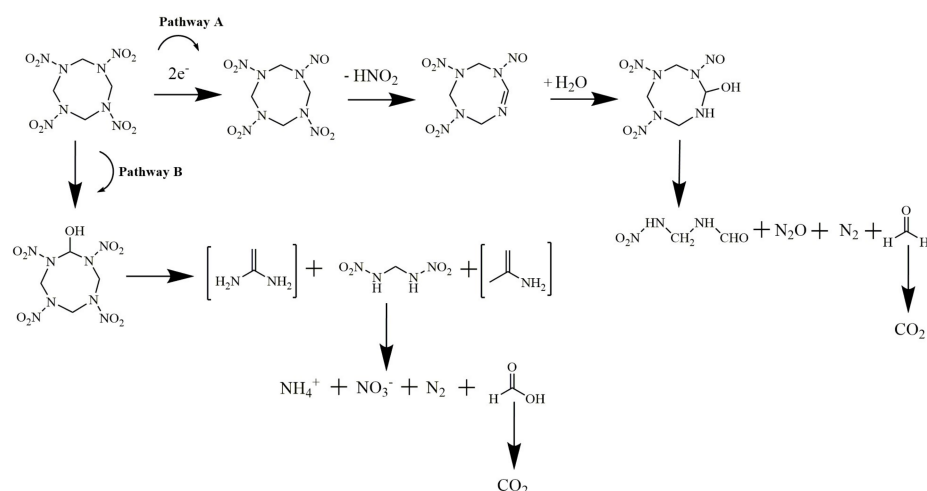


Figure 2. Possible pathways for the electrochemical degradation of HMX. Square brackets indicate undetected compounds.

To further prove the proposed pathway and evaluate the contribution of $\bullet OH$ to HMX degradation, a quenching experiment was conducted by adding tert-butanol (TBA) to the EO system. TBA is a strong $\bullet OH$ scavenger that is widely used to differentiate between direct oxidation and degradation with $\bullet OH$ radicals [60]. As shown in Figure S3, HMX removal efficiency decreased to 73.3% in the presence of 10 mM TBA. An increase in TBA concentration further inhibits HMX degradation. With the addition of 50 mM TBA, HMX removal efficiency was reduced to 48.6%. This demonstrates that indirect oxidation by $\bullet OH$ radicals (pathway B) plays an important role in HMX degradation, although cathode reduction (pathway A) or other electrocatalytic degradation mechanisms [37,61,62] will also be responsible for HMX degradation, but require further study.

2.3. Molecular-Level Toxicity Evolution during HMX Degradation

2.3.1. Molecular Toxicity Potency

A total of 114 reporter genes (Table S3) in five major stress categories (DNA stress, oxidative stress, protein stress, membrane stress, and general stress) were investigated to detect changes in their expression levels during HMX degradation. A slight increase in the overall transcriptional effect level index (TELI) value from 1.68 to 1.81 within 60 min was observed (Figure 3a), which could be attributed to the generation of relatively more toxic intermediates than HMX in the early stages of degradation. As these intermediates were further degraded to non-toxic end products (e.g., CO_2 and H_2O), the TELI values decreased, reaching a non-toxic level of 1.48 (<the threshold value of 1.5) at 180 min. According to the gene set enrichment analysis (GSEA) (Figure 3b), the main stress response pathways induced during the HMX degradation process were protein stress and oxidative stress. The

TELI_{protein} and TELI_{oxidative} reached a maximum value of 3.35 and 1.86 at 30 and 60 min, respectively. At 180 min, both values decreased to a minimum of 1.93 and 1.51, respectively.

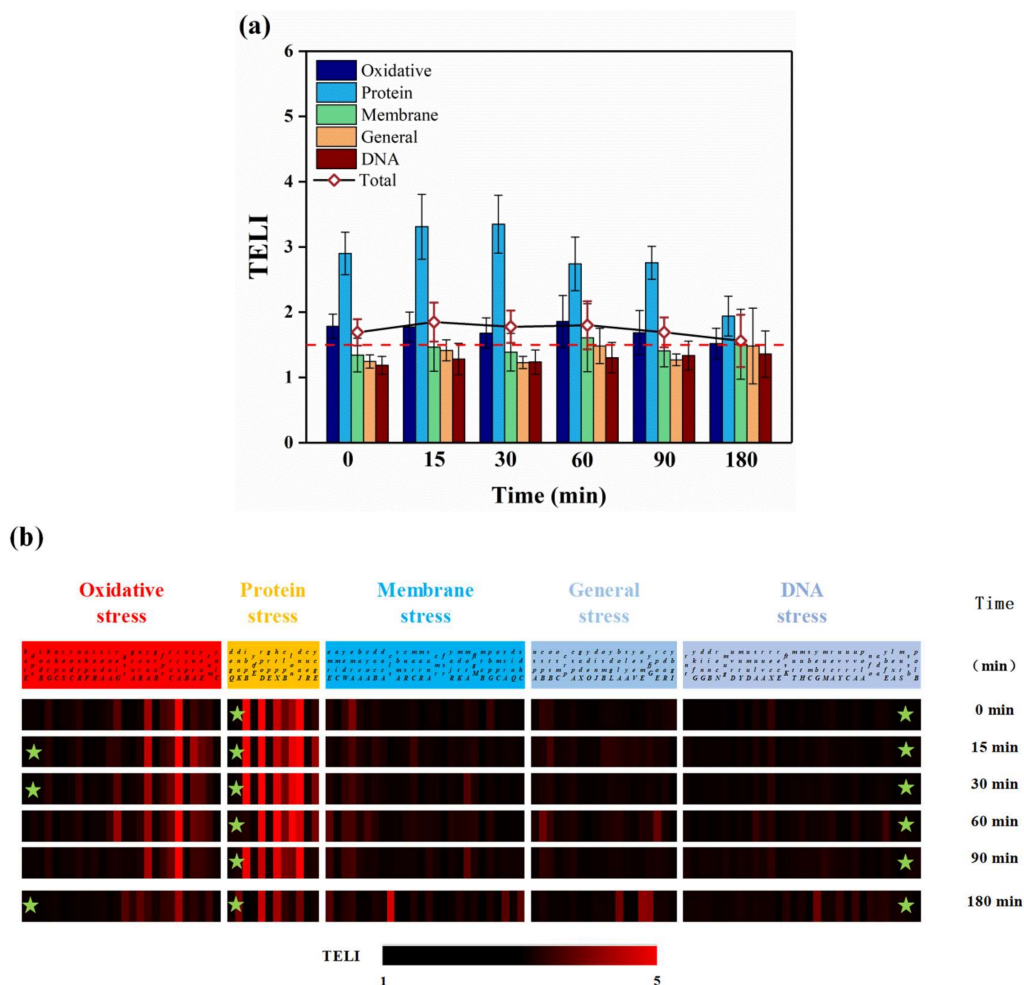


Figure 3. (a) The TELI-based toxicity profile changes during the electrochemical oxidation of HMX. (a) The TELI values for the 5 stress response categories and total TELI; (b) the TELI values for genes. The green star (★) indicates the significantly affected ($p < 0.05$) stress response categories revealed by the gene set enrichment analysis.

2.3.2. Molecular-Level Toxicity Effects

To further provide mechanistic insights into the evolution of molecular toxicity during HMX degradation, the differentially expressed genes ($TELI_{\text{gene}} > 1.5$) in the major stress categories (i.e., oxidative and protein stress) based on the TELI profiles and GSEA results were investigated (Figure 4). The number of genes showing altered expression during HMX degradation (Figure S4) increased from 24 at the initial stage to 35 at 60 min and then decreased to 30 at 180 min. Similarly, as shown in the hierarchical cluster (HCL) analysis diagram (Figure S5), the upregulated genes (e.g., *yeaE*, *zntA*, and *tam*) and downregulated genes (e.g., *yeiG*, *emrA*, *yaaA*, *fpr*, *ibpB*, *clpB*, *rpoD*, *dnaJ*, *trxA*, *lon*, *trxC*, *htpX*) were observed mainly from 0 to 90 min, whereas the altered gene expression was not significant at 180 min. These results suggest that, during the first 90 min, the degradation process produced more toxic intermediates, which could be further degraded and converted into less toxic end-products.

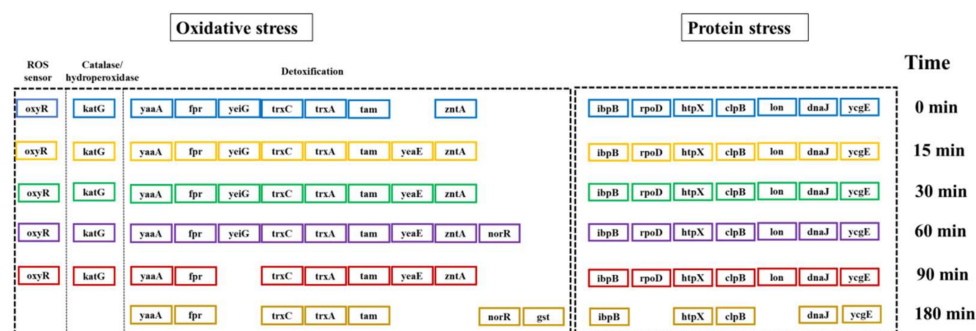


Figure 4. Major stress response pathways and biomarker genes showed altered expression ($TELI_{gene} > 1.5$) during the electrochemical oxidation of HMX. The genes were clustered into subcategories based on their functions and involvement in various pathways (Table S1).

For oxidative stress, the differential expression of reactive oxygen species (ROS) sensors, including *oxyR*, *soxR*, and *soxS*, were induced during HMX degradation. The expression of these genes in stressful environments can scavenge oxidative free radicals and resist oxidative stress [63]. Dysregulation of *oxyR* was observed from 0 to 90 min during HMX degradation, suggesting that chemical mixtures (HMX or its degradation intermediates) led to the production of cellular ROS. At the end of the test, no differential expression of ROS sensor-related genes was observed, indicating a decreased level of ROS-induced oxidative stress. We also found that the catalase/hydroperoxidase gene *katG* [64,65] was dysregulated from 0 to 90 min, indicating that H_2O_2 may be produced from O_2 at the cathode [66]. In addition, biomarkers involved in the detoxification pathway were dysregulated. For example, the *yaaA* gene, which is associated with cellular stress responses to peroxides, can be induced by the expression of the *oxyR* gene [67,68]. The *fpr* gene encoding a G protein-coupled receptor can be induced by exposure to H_2O_2 [69]. The number of dysregulated genes in the detoxification sub-pathway increased to 9 at 60 min and then decreased to 7 at 90–180 min, suggesting the generation of more toxic intermediate products, that could induce oxidative stress, at the beginning of the test, but that will further degrade to less or non-toxic end-products.

For the protein stress pathway, seven of the 12 genes showed altered expression during HMX degradation (Figure 4), whereas *rpoD* and *lon* were not perturbed at 180 min. Genes *rpoD* and *lon* regulate the synthesis of the RNA polymerase sigma factor and Lon proteases, respectively [70–72]. Lon proteases are required for the degradation of misfolded proteins. Therefore, the lack of dysregulation of those genes at 180 min indicates that the end products did not cause substantial protein misfolding.

3. Materials and Methods

3.1. Chemicals

HMX ($C_4H_8N_8O_8$, $\geq 99\%$) was obtained from Xi'an Modern Chemistry Research Institute (Xi'an, China). Sodium sulfate (Na_2SO_4 , $\geq 99\%$), sulfuric acid (H_2SO_4 , $\geq 99\%$), sodium hydroxide (NaOH pellets, $\geq 98\%$), and tert-butanol (TBA) were purchased from China National Medicines Co. Ltd. (Beijing, China). Minimal medium (M9) was purchased from Ruichu Biotechnology Co., Ltd. (Funing, China).

3.2. Experimental Design

The electrochemical reactor ($8.7 \times 9.2 \times 12$ cm, 500 mL) is shown in Figure 5. The dimensions of the Ti/PbO₂ anode and Cu cathode were 5 cm \times 10 cm and 5 cm \times 6 cm, respectively. The initial concentration of HMX was 20 mg/L. Because the performance of the EO system can be affected by various operating conditions [44], different influencing factors including Na_2SO_4 electrolyte concentrations (0.05, 0.1, 0.15, 0.2, 0.25 mol/L), applied current densities (10, 20, 30, 40, 50, and 70 mA/cm²), anode-cathode distance (0.5, 1.0, 1.5, 2.0, and 2.5 cm), and initial solution pH values (3.0, 5.0, 7.0, and 9.0) were selected for factor

analysis. The specifically detailed single-factor experimental parameter design is shown in Table S4. The levels of the different factors were selected based on a previous study by using an electrocatalytic reaction for RDX wastewater treatment [16]. The pH of the HMX wastewater was adjusted by using diluted H_2SO_4 (1 mol/L) and NaOH (1 mol/L). Samples were collected at different treatment time intervals and passed through a $0.45\ \mu\text{m}$ filter. The supernatant was stored in vials until the HMX was measured by high-performance liquid chromatography (HPLC). All samples were analyzed at least in triplicate during the experiment to measure HMX concentrations. All test solutions were collected from the supernatant, passed through a $0.45\ \mu\text{m}$ filter, and stored in vials until HPLC analysis. After determining the optimal experimental conditions, HMX wastewater was collected at different treatment times for intermediate product and toxicity analyses.

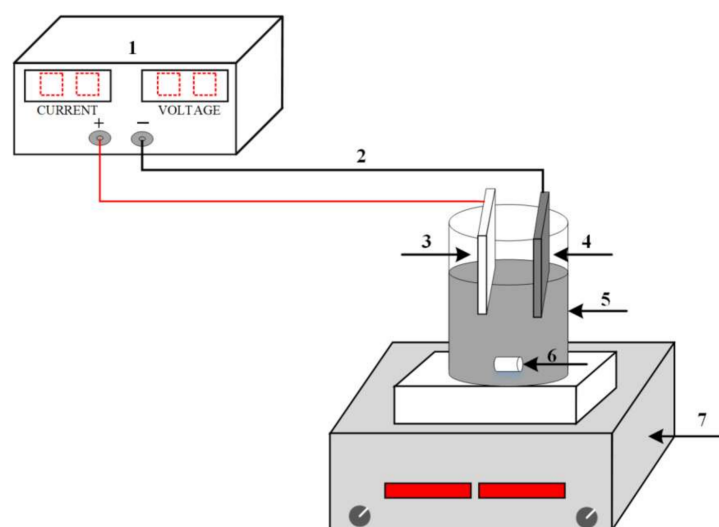


Figure 5. Electro-oxidation system for HMX wastewater treatment (1. DC power supply, 2. Copper wire, 3. Anode, 4. Cathode, 5. Electrolyte solution, 6. Rotor, 7. Magnetic stirrer).

3.3. Chemical Analysis

The concentration of HMX in the solution was determined and quantified by using HPLC (PerkinElmer, Waltham, MA, USA) and a UV detector at a flow rate of $0.7\ \text{mL}/\text{min}$. The detection wavelength of HMX was $236\ \text{nm}$ with a column temperature of $35\ ^\circ\text{C}$. The mobile phase consisted of 40% acetonitrile and 60% water (v/v). The injection volume was $20\ \mu\text{L}$. The HMX removal efficiency was calculated as Equation (1):

$$R (\%) = 1 - (C_0/C_t) \times 100\% \quad (1)$$

where C_0 and C_t are the initial and residual concentrations of HMX at different times, respectively.

The HMX degradation products were further analyzed by using LC-MS/MS. The mass spectrometer (U3000, Thermo Fisher Scientific, Waltham, MA, USA) was equipped with an electrospray ionization (ESI) source and operated in the positive ESI mode.

3.4. Radical Scavenger Experiment

To investigate the role of $\bullet\text{OH}$ in HMX degradation, TBA scavengers at different concentrations (10, 20, and 50 mM) were added to the EO system at the beginning of the test. The HMX removal efficiency was measured after 3 h, as described in Section 3.3.

3.5. Toxicity Analysis

A toxicity analysis of HMX wastewater was performed by using a library of 114 transcriptional fusions of the green fluorescent protein (GFP), which included different promoters controlling the expression of genes involved in five known stress response

pathways, namely: oxidative, DNA, protein, membrane, and general stress pathways (Table S2) in *E. coli* K12 and MG1655. A detailed toxicogenomic assay was conducted according to previous studies [32,73]. Briefly, *E. coli* cells were grown with $1 \times M9$ in clear-bottom black 384-well plates (Costar, Bethesda, MD, USA) for 5–6 h at 37 °C to reach early exponential growth (optical density value (OD_{600}) of ~0.2). Ten microliters of HMX samples at different degradation times were added to each well of the 384-well plate. The plate was then placed in a microplate reader (Cytation 5, Bio-Tek, Winooski, VT, USA) to simultaneously measure OD_{600} for cell growth and GFP signals (excitation at 485 nm, emission at 528 nm) at a time interval of 5 min for 2 h. All tests were performed in the dark and repeated three times.

3.6. Toxicogenomics Data Analysis

Gene expression profiling data from *E. coli* libraries were processed as previously described [30,57]. All the data was corrected for various controls, including a blank with medium control (with and without HMX samples) and promoterless bacterial controls (with and without HMX samples). The alteration in gene expression for a given gene at each time point, due to HMX sample exposure, relative to the vehicle control condition, without any HMX sample exposure, also referred to as induction factor I , was represented by $I = P_e/P_c$, where $P_e = (GFP/OD)_{\text{experiment}}$ as the normalized gene expression GFP level in the experimental condition with HMX sample exposure and $P_c = (GFP/OD)_{\text{vehicle}}$ in the vehicle control condition without any HMX sample exposure.

The quantitative molecular endpoint, the TELI, was calculated by integrating the temporal dysregulation of I values over the exposure time, as previously described [30,57]. A TELI value above the threshold of 1.5 was considered toxicity-positive [73].

3.7. Cost Estimation

To evaluate the application potential of EO systems, the energy consumption (EC) analysis was conducted based on Equation (2) [74],

$$\text{Electrical energy consumption (kwh/g)} = U_{\text{cell}} \frac{IT}{V * (C_t - C_0)}, \quad (2)$$

where U_{cell} is the average of applied voltage (V), I is the current (A), T is the time (h), V is the sample volume (L), C_0 and C_t are the initial and residual concentrations of HMX at different times.

3.8. Data Processing

Bar and scatter plots were drawn by using the Origin 2021 software (OriginLab Corporation, Northampton, MA, USA). Red, black, and green heat maps were plotted in Excel 2016 (Microsoft, Redmond, WA, USA). To assess the activity of stress categories or genes, gene set enrichment analysis (GSEA) was performed by sorting the gene list by TELI values, as described by Subramanian et al. [75]. For each stress response category, GSEA calculates the enrichment score; that is, it examines the genes sorted by TELI from highest to lowest, and gives a positive statistical value (i.e., rewarding score) if the gene belongs to the pathway of interest; otherwise, it gives a negative score (i.e., penalizing score). The significance of each pathway ($p < 0.05$) was determined by comparing its ranking score with the corresponding empirical distribution.

4. Conclusions

This study demonstrated that an EO system with a Ti/PbO₂ electrode can be employed for HMX wastewater treatment. The highest HMX removal efficiency of 81.2% was achieved within 180 min at a current density of 70 mA/cm², Na₂SO₄ concentration of 0.25 mol/L, interelectrode distance of 1.0 cm, and pH of 5.0. The degradation intermediates of the HMX wastewater suggest two possible electrochemical pathways: cathode reduction and indirect oxidation by •OH radicals. Protein and oxidative stress were the

key stress categories in HMX wastewater. The intermediates generated during the first 90 min of degradation had relatively higher molecular toxicity levels and were then gradually converted to less toxic or non-toxic end-products. Our study provides new insights into performance optimization, degradation pathways, and molecular-level toxicity evolution during HMX degradation. More extensive studies regarding electrode material development, EO reaction mechanisms, and potential health risks of real wastewater are needed for an in-depth and comprehensive understanding of EO-enabled methods, and for developing a promising explosive wastewater treatment method with high removal performance and low environmental impact.

Supplementary Materials: The following supporting information can be downloaded at <https://www.mdpi.com/article/10.3390/catal12080815/s1>, Figure S1: (a) The energy consumption (EC) at different (a) electrolyte concentration, (b) current density, (c) interelectrode, and (d) initial pH; Figure S2: Ion spectra of HMX degradation intermediates in positive ion mode; Figure S3: Removal of HMX under optimal conditions in the presence of different TBA concentrations; Figure S4: The number of genes showing altered expression ($TELL_{\text{gene}} > 1.5$) during the electrochemical oxidation of HMX; Figure S5: Hierarchical cluster (HCL) analysis diagram based on differential gene expressions (mean $\ln I$, $n = 3$) of 114 selected stress genes in *E. coli* in exposure to the HMX samples at different times (Red colors indicate up-regulation, green colors indicate down-regulation); Table S1: Kinetics and energy consumption of HMX degradation under different operating conditions.; Table S2. Main degradation intermediates of HMX; Table S3: Stress gene bank and its main functions; Table S4: Single-factor experimental design.

Author Contributions: Conceptualization, Y.Q.; methodology, Y.Q. and D.W.; software, K.C.; validation, Y.Q. and K.C.; formal analysis, G.C. and P.X.; investigation, Y.Q., K.C. and G.C.; resources, P.X.; data curation, H.Y., L.Q. and L.X.; writing—original draft preparation, Y.Q.; writing—review and editing, W.Y. and D.W.; visualization, X.L. and Y.L.; supervision, W.Y. and D.W.; funding acquisition, D.W. All authors have read and agreed to the published version of the manuscript.

Funding: This research was funded by the National Natural Science Foundation of China (grant number: 52070156; 31600421). Scientific Research Program Funded by Shaanxi Provincial Education Department (No. 17JS097).

Data Availability Statement: Not applicable.

Conflicts of Interest: The authors declare no conflict of interest. The funders had no role in the study design, collection, analyses, or interpretation of the data, writing of the manuscript, or decision to publish the results.

References

1. Lyman, J.L.; Liau, Y.-C.; Brand, H.V. Thermochemical functions for gas-phase, 1, 3, 5, 7-tetranitro-1, 3, 5, 7-tetraazacyclooctane (HMX), its condensed phases, and its larger reaction products. *Combust. Flame* **2002**, *130*, 185–203. [[CrossRef](#)]
2. Yang, X.; Lai, J.-l.; Li, J.; Zhang, Y.; Luo, X.-G.; Han, M.-W.; Zhu, Y.-B.; Zhao, S.-P. Biodegradation and physiological response mechanism of *Bacillus aryabhatai* to cyclotetramethylenete-tranitramine (HMX) contamination. *J. Environ. Manag.* **2021**, *288*, 112247. [[CrossRef](#)] [[PubMed](#)]
3. McMurry, S.T.; Jones, L.E.; Smith, P.; Cobb, G.; Anderson, T.; Lovern, M.B.; Cox, S.; Pan, X. Accumulation and effects of octahydro-1,3,5,7-tetranitro-1,3,5,7-tetrazocine (HMX) exposure in the green anole (*Anolis carolinensis*). *Ecotoxicology* **2012**, *21*, 304–314. [[CrossRef](#)]
4. USEPA. *Integrated Risk Information System (IRIS)*; Chemical Assessment Summary; USEPA: Washington, DC, USA, 2016.
5. Savard, K.; Berthelot, Y.; Auroy, A.; Spear, P.A.; Trottier, B.; Robidoux, P.Y. Effects of HMX-lead mixtures on reproduction of the earthworm *Eisenia Andrei*. *Arch. Environ. Contam. Toxicol.* **2007**, *53*, 351–358. [[CrossRef](#)] [[PubMed](#)]
6. Gong, P.; Hawari, J.; Thiboutot, S.; Ampleman, G.; Sunahara, G. Toxicity of octahydro-1, 3, 5, 7-tetranitro-1, 3, 5, 7-tetrazocine (HMX) to soil microbes. *Bull. Environ. Contam. Toxicol.* **2002**, *69*, 97–103. [[CrossRef](#)] [[PubMed](#)]
7. Payne, Z.M.; Lamichhane, K.M.; Babcock, R.W.; Turnbull, S.J. Pilot-scale in situ bioremediation of HMX and RDX in soil pore water in Hawaii. *Environ. Sci. Processes Impacts* **2013**, *15*, 2023–2029. [[CrossRef](#)] [[PubMed](#)]
8. Panja, S.; Sarkar, D.; Datta, R. Vetiver grass (*Chrysopogon zizanioides*) is capable of removing insensitive high explosives from munition industry wastewater. *Chemosphere* **2018**, *209*, 920–927. [[CrossRef](#)]
9. Adrian, N.R.; Arnett, C.M. Anaerobic biodegradation of hexahydro-1,3,5-trinitro-1,3,5-triazine (RDX) by *Acetobacterium malicum* strain HAAP-1 isolated from a methanogenic mixed culture. *Curr. Microbiol.* **2004**, *48*, 332–340. [[CrossRef](#)]

10. Bhatt, M.; Zhao, J.-S.; Monteil-Rivera, F.; Hawari, J. Biodegradation of cyclic nitramines by tropical marine sediment bacteria. *J. Ind. Microbiol. Biotechnol.* **2005**, *32*, 261–267. [[CrossRef](#)]
11. Singh, R.; Singh, A. Biodegradation of military explosives RDX and HMX. In *Microbial Degradation of Xenobiotics*; Springer: Berlin/Heidelberg, Germany, 2012; pp. 235–261.
12. Zhao, J.-S.; Greer, C.W.; Thiboutot, S.; Ampleman, G.; Hawari, J. Biodegradation of the nitramine explosives hexahydro-1, 3, 5-trinitro-1,3,5-triazine and octahydro-1,3,5,7-tetranitro-1,3,5,7-tetrazocine in cold marine sediment under anaerobic and oligotrophic conditions. *Can. J. Microbiol.* **2004**, *50*, 91–96. [[CrossRef](#)]
13. Kanekar, S.; Kanekar, P.; Sarnaik, S.; Gujrathi, N.; Shede, P.; Kedargol, M.; Reardon, K. Bioremediation of nitroexplosive wastewater by an yeast isolate *Pichia sydowiorum* MCM Y-3 in fixed film bioreactor. *J. Ind. Microbiol. Biotechnol.* **2009**, *36*, 253–260. [[CrossRef](#)] [[PubMed](#)]
14. Shang, K.; Wang, X.; Li, J.; Wang, H.; Lu, N.; Jiang, N.; Wu, Y. Synergetic degradation of Acid Orange 7 (AO7) dye by DBD plasma and persulfate. *Chem. Eng. J.* **2017**, *311*, 378–384. [[CrossRef](#)]
15. Wang, L.; Luo, Z.; Hong, Y.; Chelme-Ayala, P.; Meng, L.; Wu, Z.; El-Din, M.G. The treatment of electroplating wastewater using an integrated approach of interior microelectrolysis and Fenton combined with recycle ferrite. *Chemosphere* **2022**, *286*, 131543. [[CrossRef](#)]
16. Chen, Y.; Hong, L.; Han, W.; Wang, L.; Sun, X.; Li, J. Treatment of high explosive production wastewater containing RDX by combined electrocatalytic reaction and anoxic–oxic biodegradation. *Chem. Eng. J.* **2011**, *168*, 1256–1262. [[CrossRef](#)]
17. Moreira, F.C.; Boaventura, R.A.; Brillas, E.; Vilar, V.J. Electrochemical advanced oxidation processes: A review on their application to synthetic and real wastewaters. *Appl. Catal. B Environ.* **2017**, *202*, 217–261. [[CrossRef](#)]
18. Martinez-Huitle, C.A.; Ferro, S. Electrochemical oxidation of organic pollutants for the wastewater treatment: Direct and indirect processes. *Chem. Soc. Rev.* **2006**, *35*, 1324–1340. [[CrossRef](#)]
19. Panizza, M.; Cerisola, G. Direct and mediated anodic oxidation of organic pollutants. *Chem. Rev.* **2009**, *109*, 6541–6569. [[CrossRef](#)]
20. Oturan, M.A.; Aaron, J.-J. Advanced oxidation processes in water/wastewater treatment: Principles and applications. A review. *Crit. Rev. Environ. Sci. Technol.* **2014**, *44*, 2577–2641. [[CrossRef](#)]
21. Moreira, F.C.; Soler, J.; Fonseca, A.; Saraiva, I.; Boaventura, R.A.; Brillas, E.; Vilar, V.J. Incorporation of electrochemical advanced oxidation processes in a multistage treatment system for sanitary landfill leachate. *Water Res.* **2015**, *81*, 375–387. [[CrossRef](#)]
22. Dai Lam, T.; Van Chat, N.; Bach, V.Q.; Loi, V.D.; Van Anh, N. Simultaneous degradation of 2,4,6-trinitrophenyl-N-methylnitramine (Tetryl) and hexahydro-1,3,5-trinitro-1,3,5 triazine (RDX) in polluted wastewater using some advanced oxidation processes. *J. Ind. Eng. Chem.* **2014**, *20*, 1468–1475.
23. Bonin, P.M.; Bejan, D.; Radovic-Hrapovic, Z.; Halasz, A.; Hawari, J.; Bunce, N.J. Indirect oxidation of RDX, HMX, and CL-20 cyclic nitramines in aqueous solution at boron-doped diamond electrodes. *Environ. Chem.* **2005**, *2*, 125–129. [[CrossRef](#)]
24. Kacem, S.B.; Elaoud, S.C.; Asensio, A.M.; Panizza, M.; Clematis, D. Electrochemical and sonoelectrochemical degradation of Allura Red and Erythrosine B dyes with Ti-PbO₂ anode. *J. Electroanal. Chem.* **2021**, *889*, 115212. [[CrossRef](#)]
25. Song, S.; Zhan, L.; He, Z.; Lin, L.; Tu, J.; Zhang, Z.; Chen, J.; Xu, L. Mechanism of the anodic oxidation of 4-chloro-3-methyl phenol in aqueous solution using Ti/SnO₂-Sb/PbO₂ electrodes. *J. Hazard. Mater.* **2010**, *175*, 614–621. [[CrossRef](#)] [[PubMed](#)]
26. Suryanarayanan, V.; Nakazawa, I.; Yoshihara, S.; Shirakashi, T. The influence of electrolyte media on the deposition/dissolution of lead dioxide on boron-doped diamond electrode—A surface morphologic study. *J. Electroanal. Chem.* **2006**, *592*, 175–182. [[CrossRef](#)]
27. García-Gómez, C.; Drogui, P.; Seyhi, B.; Gortáres-Moroyoqui, P.; Buelna, G.; Estrada-Alvargado, M.; Alvarez, L.H. Combined membrane bioreactor and electrochemical oxidation using Ti/PbO₂ anode for the removal of carbamazepine. *J. Taiwan Inst. Chem. Eng.* **2016**, *64*, 211–219. [[CrossRef](#)]
28. Wang, J.; Wang, N.; Nan, W.; Wang, C.; Chen, X.; Qi, X.; Yan, S.; Dai, S. Enhancement of electrochemical performance of LiCoO₂ cathode material at high cut-off voltage (4.5 V) by partial surface coating with graphene nanosheets. *Int. J. Electrochem. Sci.* **2020**, *15*, 9282–9293.
29. Zhao, J.-S.; Spain, J.; Thiboutot, S.; Ampleman, G.; Greer, C.; Hawari, J. Phylogeny of cyclic nitramine-degrading psychrophilic bacteria in marine sediment and their potential role in the natural attenuation of explosives. *FEMS Microbiol. Ecol.* **2004**, *49*, 349–357. [[CrossRef](#)]
30. Hawari, J.; Halasz, A.; Beaudet, S.; Paquet, L.; Ampleman, G.; Thiboutot, S. Biotransformation routes of octahydro-1, 3, 5, 7-tetranitro-1, 3, 5, 7-tetrazocine by municipal anaerobic sludge. *Environ. Sci. Technol.* **2001**, *35*, 70–75. [[CrossRef](#)]
31. Mukhi, S.; Patiño, R. Effects of hexahydro-1,3,5-trinitro-1,3,5-triazine (RDX) in zebrafish: General and reproductive toxicity. *Chemosphere* **2008**, *72*, 726–732. [[CrossRef](#)]
32. Nipper, M.; Carr, R.; Biedenbach, J.; Hooten, R.; Miller, K.; Saepoff, S. Development of marine toxicity data for ordnance compounds. *Arch. Environ. Contam. Toxicol.* **2001**, *41*, 308–318. [[CrossRef](#)]
33. Gou, N.; Onnis-Hayden, A.; Gu, A.Z. Mechanistic toxicity assessment of nanomaterials by whole-cell-array stress genes expression analysis. *Environ. Sci. Technol.* **2010**, *44*, 5964–5970. [[CrossRef](#)]
34. Lin, Y.; Sevillano-Rivera, M.; Jiang, T.; Li, G.; Cotto, I.; Vosloo, S.; Carpenter, C.M.; Larese-Casanova, P.; Giese, R.W.; Helbling, D.E. Impact of Hurricane Maria on drinking water quality in Puerto Rico. *Environ. Sci. Technol.* **2020**, *54*, 9495–9509. [[CrossRef](#)] [[PubMed](#)]
35. El-Desoky, H.S.; Ghoneim, M.M.; Zidan, N.M. Decolorization and degradation of Ponceau S azo-dye in aqueous solutions by the electrochemical advanced Fenton oxidation. *Desalination* **2010**, *264*, 143–150. [[CrossRef](#)]

36. Dai, Q.; Zhou, J.; Weng, M.; Luo, X.; Feng, D.; Chen, J. Electrochemical oxidation metronidazole with Co modified PbO₂ electrode: Degradation and mechanism. *Sep. Purif. Technol.* **2016**, *166*, 109–116. [[CrossRef](#)]
37. Samarghandi, M.R.; Ansari, A.; Dargahi, A.; Shabanloo, A.; Nematollahi, D.; Khazaei, M.; Nasab, H.Z.; Vaziri, Y. Enhanced electrocatalytic degradation of bisphenol A by graphite/ β -PbO₂ anode in a three-dimensional electrochemical reactor. *J. Environ. Chem. Eng.* **2021**, *9*, 106072. [[CrossRef](#)]
38. Wang, Y.; Shen, Z.; Chen, X. Effects of experimental parameters on 2,4-dichlorophenol degradation over Er-chitosan-PbO₂ electrode. *J. Hazard. Mater.* **2010**, *178*, 867–874. [[CrossRef](#)] [[PubMed](#)]
39. Klidi, N.; Clematis, D.; Delucchi, M.; Gadri, A.; Ammar, S.; Panizza, M. Applicability of electrochemical methods to paper mill wastewater for reuse. Anodic oxidation with BDD and TiRuSnO₂ anodes. *J. Electroanal. Chem.* **2018**, *815*, 16–23. [[CrossRef](#)]
40. Zhu, X.; Hu, W.; Feng, C.; Chen, N.; Chen, H.; Kuang, P.; Deng, Y.; Ma, L. Electrochemical oxidation of aniline using Ti/RuO₂-SnO₂ and Ti/RuO₂-IrO₂ as anode. *Chemosphere* **2021**, *269*, 128734. [[CrossRef](#)]
41. Shi, H.; Wang, Q.; Ni, J.; Xu, Y.; Song, N.; Gao, M. Highly efficient removal of amoxicillin from water by three-dimensional electrode system within granular activated carbon as particle electrode. *J. Water Process Eng.* **2020**, *38*, 101656. [[CrossRef](#)]
42. Wu, H.; Xie, H.; He, G.; Guan, Y.; Zhang, Y. Effects of the pH and anions on the adsorption of tetracycline on iron-montmorillonite. *Appl. Clay Sci.* **2016**, *119*, 161–169. [[CrossRef](#)]
43. Zaky, A.M.; Chaplin, B.P. Mechanism of p-substituted phenol oxidation at a Ti4O7 reactive electrochemical membrane. *Environ. Sci. Technol.* **2014**, *48*, 5857–5867. [[CrossRef](#)]
44. Zhang, J.; Zhou, Y.; Yao, B.; Yang, J.; Zhi, D. Current progress in electrochemical anodic-oxidation of pharmaceuticals: Mechanisms, influencing factors, and new technique. *J. Hazard. Mater.* **2021**, *418*, 126313. [[CrossRef](#)] [[PubMed](#)]
45. Liou, M.-J.; Lu, M.-C.; Chen, J.-N. Oxidation of explosives by Fenton and photo-Fenton processes. *Water Res.* **2003**, *37*, 3172–3179. [[CrossRef](#)]
46. Xiang, H.; Xiao, S.; Zhang, G.; Song, Y.; Cui, P.; Shao, H.; Li, H. Treatment of simulated berberine pharmaceutical wastewater by electrochemical oxidation process. *J. Environ. Eng.* **2011**, *5*, 5.
47. Lin, H.; Niu, J.; Xu, J.; Li, Y.; Pan, Y. Electrochemical mineralization of sulfamethoxazole by Ti/SnO₂-Sb/Ce-PbO₂ anode: Kinetics, reaction pathways, and energy cost evolution. *Electrochim. Acta* **2013**, *97*, 167–174. [[CrossRef](#)]
48. Lei, L.; Dai, Q.; Zhou, M.; Zhang, X. Decolorization of cationic red X-GRL by wet air oxidation: Performance optimization and degradation mechanism. *Chemosphere* **2007**, *68*, 1135–1142. [[CrossRef](#)]
49. Radha, K.; Sridevi, V.; Kalaivani, K. Electrochemical oxidation for the treatment of textile industry wastewater. *Bioresour. Technol.* **2009**, *100*, 987–990. [[CrossRef](#)]
50. Dargahi, A.; Barzoki, H.R.; Vosoughi, M.; Mokhtari, S.A. Enhanced electrocatalytic degradation of 2, 4-Dinitrophenol (2, 4-DNP) in three-dimensional sono-electrochemical (3D/SEC) process equipped with Fe/SBA-15 nanocomposite particle electrodes: Degradation pathway and application for real wastewater. *Arab. J. Chem.* **2022**, *15*, 103801. [[CrossRef](#)]
51. Li, X.; Li, X.; Yang, W.; Chen, X.; Li, W.; Luo, B.; Wang, K. Preparation of 3D PbO₂ nanospheres@SnO₂ nanowires/Ti electrode and its application in methyl orange degradation. *Electrochim. Acta* **2014**, *146*, 15–22. [[CrossRef](#)]
52. Neto, S.A.; De Andrade, A. Electrooxidation of glyphosate herbicide at different DSA[®] compositions: pH, concentration and supporting electrolyte effect. *Electrochim. Acta* **2009**, *54*, 2039–2045. [[CrossRef](#)]
53. Dargahi, A.; Vosoughi, M.; Mokhtari, S.A.; Vaziri, Y.; Alighadri, M. Electrochemical degradation of 2, 4-Dinitrotoluene (DNT) from aqueous solutions using three-dimensional electrocatalytic reactor (3DER): Degradation pathway, evaluation of toxicity and optimization using RSM-CCD. *Arab. J. Chem.* **2022**, *15*, 103648. [[CrossRef](#)]
54. Rahmani, A.; Leili, M.; Seid-Mohammadi, A.; Shabanloo, A.; Ansari, A.; Nematollahi, D.; Alizadeh, S. Improved degradation of diuron herbicide and pesticide wastewater treatment in a three-dimensional electrochemical reactor equipped with PbO₂ anodes and granular activated carbon particle electrodes. *J. Clean. Prod.* **2021**, *322*, 129094. [[CrossRef](#)]
55. Li, C.; Xiong, K.; Li, D.; Liang, J.; Guo, B. Experimental study on treatment of antibiotic pharmaceutical wastewater by electrocatalytic oxidation. *Environ. Prot. Circ. Econ.* **2017**, *37*, 5.
56. Shao, D.; Wang, Z.; Zhang, C.; Li, W.; Xu, H.; Tan, G.; Yan, W. Embedding wasted hairs in Ti/PbO₂ anode for efficient and sustainable electrochemical oxidation of organic wastewater. *Chin. Chem. Lett.* **2022**, *33*, 1288–1292. [[CrossRef](#)]
57. Crocker, F.H.; Indest, K.J.; Fredrickson, H.L. Biodegradation of the cyclic nitramine explosives RDX, HMX, and CL-20. *Appl. Microbiol. Biotechnol.* **2006**, *73*, 274–290. [[CrossRef](#)] [[PubMed](#)]
58. Fournier, D.; Halasz, A.; Thiboutot, S.; Ampleman, G.; Manno, D.; Hawari, J. Biodegradation of octahydro-1,3,5,7-tetranitro-1,3,5,7-tetrazocine (HMX) by Phanerochaete chrysosporium: New insight into the degradation pathway. *Environ. Sci. Technol.* **2004**, *38*, 4130–4133. [[CrossRef](#)] [[PubMed](#)]
59. Anotai, J.; Tanvanit, P.; Garcia-Segura, S.; Lu, M.-C. Electro-assisted Fenton treatment of ammunition wastewater containing nitramine explosives. *Process Saf. Environ. Prot.* **2017**, *109*, 429–436. [[CrossRef](#)]
60. Dugandžić, A.M.; Tomašević, A.V.; Radišić, M.M.; Šekuljica, N.Ž.; Mijjin, D.Ž.; Petrović, S.D. Effect of inorganic ions, photosensitisers and scavengers on the photocatalytic degradation of nicosulfuron. *J. Photochem. Photobiol. A Chem.* **2017**, *336*, 146–155. [[CrossRef](#)]
61. Sun, W.; Sun, Y.; Shah, K.J.; Chiang, P.-C.; Zheng, H. Electrocatalytic oxidation of tetracycline by Bi-Sn-Sb/ γ -Al₂O₃ three-dimensional particle electrode. *J. Hazard. Mater.* **2019**, *370*, 24–32. [[CrossRef](#)]

62. Yang, J.-S.; Lai, W.W.-P.; Panchangam, S.C.; Lin, A.Y.-C. Photoelectrochemical degradation of perfluorooctanoic acid (PFOA) with GOP25/FTO anodes: Intermediates and reaction pathways. *J. Hazard. Mater.* **2020**, *391*, 122247. [[CrossRef](#)]
63. Keseler, I.M.; Bonavides-Martínez, C.; Collado-Vides, J.; Gama-Castro, S.; Gunsalus, R.P.; Johnson, D.A.; Krummenacker, M.; Nolan, L.M.; Paley, S.; Paulsen, I.T. EcoCyc: A comprehensive view of *Escherichia coli* biology. *Nucleic Acids Res.* **2009**, *37*, D464–D470. [[CrossRef](#)]
64. Seaver, L.C.; Imlay, J.A. Alkyl hydroperoxide reductase is the primary scavenger of endogenous hydrogen peroxide in *Escherichia coli*. *J. Bacteriol.* **2001**, *183*, 7173–7181. [[CrossRef](#)] [[PubMed](#)]
65. Seaver, L.C.; Imlay, J.A. Hydrogen peroxide fluxes and compartmentalization inside growing *Escherichia coli*. *J. Bacteriol.* **2001**, *183*, 7182–7189. [[CrossRef](#)] [[PubMed](#)]
66. Yeager, E. Electrocatalysts for O₂ reduction. *Electrochim. Acta* **1984**, *29*, 1527–1537. [[CrossRef](#)]
67. Zheng, M.; Wang, X.; Templeton, L.J.; Smulski, D.R.; LaRossa, R.A.; Storz, G. DNA microarray-mediated transcriptional profiling of the *Escherichia coli* response to hydrogen peroxide. *J. Bacteriol.* **2001**, *183*, 4562–4570. [[CrossRef](#)]
68. Liu, Y.; Bauer, S.C.; Imlay, J.A. The YaaA protein of the *Escherichia coli* OxyR regulon lessens hydrogen peroxide toxicity by diminishing the amount of intracellular unincorporated iron. *J. Bacteriol.* **2011**, *193*, 2186–2196. [[CrossRef](#)]
69. Manchado, M.; Michán, C.; Pueyo, C. Hydrogen peroxide activates the SoxRS regulon in vivo. *J. Bacteriol.* **2000**, *182*, 6842–6844. [[CrossRef](#)]
70. Burgess, R.R.; Travers, A.A.; Dunn, J.J.; Bautz, E.K. Factor stimulating transcription by RNA polymerase. *Nature* **1969**, *221*, 43–46. [[CrossRef](#)]
71. Rosen, R.; Biran, D.; Gur, E.; Becher, D.; Hecker, M.; Ron, E.Z. Protein aggregation in *Escherichia coli*: Role of proteases. *FEMS Microbiol. Lett.* **2002**, *207*, 9–12. [[CrossRef](#)]
72. Shineberg, B.; Zipser, D. The lon gene and degradation of β -galactosidase nonsense fragments. *J. Bacteriol.* **1973**, *116*, 1469–1471. [[CrossRef](#)]
73. Gou, N.; Gu, A.Z. A new transcriptional effect level index (TELI) for toxicogenomics-based toxicity assessment. *Environ. Sci. Technol.* **2011**, *45*, 5410–5417. [[CrossRef](#)]
74. Zeng, Q.; Zan, F.; Hao, T.; Biswal, B.K.; Lin, S.; van Loosdrecht, M.C.; Chen, G. Electrochemical pretreatment for stabilization of waste activated sludge: Simultaneously enhancing dewaterability, inactivating pathogens and mitigating hydrogen sulfide. *Water Res.* **2019**, *166*, 115035. [[CrossRef](#)] [[PubMed](#)]
75. Subramanian, A.; Tamayo, P.; Mootha, V.K.; Mukherjee, S.; Ebert, B.L.; Gillette, M.A.; Paulovich, A.; Pomeroy, S.L.; Golub, T.R.; Lander, E.S. Gene set enrichment analysis: A knowledge-based approach for interpreting genome-wide expression profiles. *Proc. Natl. Acad. Sci. USA* **2005**, *102*, 15545–15550. [[CrossRef](#)] [[PubMed](#)]